Linking the micro and macro: L-H transition dynamics and threshold physics

M. A. Malkov, P. H. Diamond, K. Miki, J. E. Rice, and G. R. Tynan

---

Articles you may be interested in

Simulations of the L-H transition on experimental advanced superconducting Tokamak
Phys. Plasmas 21, 122501 (2014); 10.1063/1.4901597

Direct observations of L-I-H and H-I-L transitions with the X-point reciprocating probe in ASDEX Upgrade
Phys. Plasmas 21, 042301 (2014); 10.1063/1.4870012

Gyrokinetic simulations of reverse shear Alfvén eigenmodes in DIII-D plasmas
Phys. Plasmas 20, 012109 (2013); 10.1063/1.4775776

Collisional damping for ion temperature gradient mode driven zonal flow
Phys. Plasmas 14, 032302 (2007); 10.1063/1.2536297

Analysis of metallic impurity density profiles in low collisionality Joint European Torus H-mode and L-mode plasmas
Phys. Plasmas 13, 042501 (2006); 10.1063/1.2187424

Linking the micro and macro: L-H transition dynamics and threshold physics

M. A. Malkov,[1,a)] P. H. Diamond,[1] K. Miki,[2] J. E. Rice,[3] and G. R. Tynan[4]

[1]CASS and Department of Physics, University of California, San Diego, California 92093, USA
[2]JAEA, Kashiwa, Japan
[3]Plasma Science and Fusion Center, MIT, Cambridge, Massachusetts 02139, USA
[4]Center for Momentum Transport and Flow Organization, University of California, San Diego, California 92093, USA

The links between the microscopic dynamics and macroscopic threshold physics of the L → H transition are elucidated. Emphasis is placed on understanding the physics of power threshold scalings, and especially on understanding the *minimum in the power threshold* as a function of density $P_{thr}(n)$. By extending a numerical 1D model to evolve both electron and ion temperatures, including collisional coupling, we find that the decrease in $P_{thr}(n)$ along the low-density branch is due to the combination of an increase in collisional electron-to-ion energy transfer and an increase in the heating fraction coupled to the ions. Both processes strengthen the edge diamagnetic electric field needed to lock in the mean electric field shear for the L → H transition. The increase in $P_{thr}(n)$ along the high-density branch is due to the increase with ion collisionality of damping of turbulence-driven shear flows. Turbulence driven shear flows are needed to trigger the transition by extracting energy from the turbulence. Thus, we identify the critical transition physics components of the separatrix ion heat flux and the zonal flow excitation. The model reveals a power threshold minimum in density scans as a crossover between the threshold decrease supported by an increase in heat fraction received by ions (directly or indirectly, from electrons) and a threshold increase, supported by the rise in shear flow damping. The electron/ion heating mix emerges as important to the transition, in that it, together with electron-ion coupling, regulates the edge diamagnetic electric field shear. The importance of possible collisionless electron-ion heat transfer processes is explained. © 2015 AIP Publishing LLC. [http://dx.doi.org/10.1063/1.4914934]

I. INTRODUCTION

Good confinement is critical to ITER ignition. The preferred route to good confinement is the high confinement mode, or H-mode. The H-mode, as opposed to the low-confinement, or L-mode, is characterized by the spontaneous buildup of steep density and pressure gradients at the plasma edge. There is mounting evidence that L → H transition is triggered by turbulence energy coupling to low frequency shear flows via Reynolds work.[1-18] As a consequence, turbulence and turbulent transport collapse, enabling the increase of the edge diamagnetic electric field shear (associated with the pressure gradient $\nabla \langle P \rangle$) and thus the ultimate L → H transition and the development of an edge transport barrier (ETB). This evolution can occur via an extended cyclic I-phase or in a single burst of shear flow growth.[19-21] Recent fluctuation measurements[16] and transition model studies[22] support this two-step scenario. However, the improved understanding of dynamics so far has not yielded an improved understanding of the power threshold. This is critical, as power remains the principal macroscopic control knob on the transition.

Early models of the L-H transition were phenomenological and concentrated on the transition power threshold scaling in density n and magnetic field B_T. A simple power-law $P_{thr} \sim n^x B_T^y$ was commonly used, with the scaling exponents x for n and y for B_T extracted from empirical scans. The scaling exponents were estimated from the multi-machine fits,[23]

which typically placed both exponents in the range 0.7–0.8. Another phenomenological approach was suggested by Wagner (e.g., Ref. 24) and was based on a requirement that the ion diamagnetic velocity $V_{di} = -(c/enB)\partial P_i/\partial r$ exceeds a critical value for the transition to occur. Of course, V_{di} is a component of the $\mathbf{E} \times \mathbf{B}$ velocity, as well. This yielded $P_{thr} \propto nB$, and the critical value for the velocity was obtained from the measurement of the electron pressure gradient at the transition point.

Simple power threshold scalings are obviously inconsistent with the well known minimum in the $P_{thr}(n)$ curve, long observed in many tokamaks[25] (see Ref. 26 for a review). The observations are not easy to interpret because of the significant data point scatter and variations between different machines. These differences are concerned with both the depth of the minimum and the density at the minimum point, which cannot be explained merely by variations in magnetic field.[27] The $P_{thr}(n) \propto n^{0.7}$ scaling inferred from experiments is relevant only to the high-density branch of the $P_{thr}(n)$-curve and yields no additional insight into the nature of the minimum. Dedicated experimental studies, particularly the recent papers[27,28] indicate that electron heating—especially electron cyclotron heating (ECH)—combined with inefficient collisional electron-ion heat exchange on the low-density branch are crucial to the threshold minimum.

Going beyond phenomenology, the difficulties in understanding threshold physics are the mesoscale and multistage characters of L → H phenomena, which involve coupling the

a)E-mail: mmalkov@ucsd.edu

turbulence-driven and mean flows to small scale turbulence that also determines the pressure and density gradients. These gradients drive the turbulence and must be evolved dynamically. Given the complexity of these feed-back loops, the key physical dependencies of the L → H transition are difficult to determine from the *ab-initio* numerical simulations. This motivated the development of simplified, low-degree-of-freedom models, such as the simple 0D model of the L → H transition suggested in Refs. 3 and 29. This was supported experimentally, e.g., Refs. 11 and 30 and followed up by theoretical development and improved models.[31–33]

A further advance of the 0D model was its 1D, five-field extension[10] which, in addition to the drift wave (DW) intensity and zonal flow (ZF) energy, also evolved the mean flow (MF), pressure, and density. Using this model, important new signatures of the transition were recovered and documented in Refs. 10, 22, 34, and 35. In particular, a strong mean flow jet, tightly collimated at the edge, was identified as a robust mesoscale signal of LH transition. Of course, such features of the flow are beyond the reach of 0D models.

Here, we proceed to study the threshold physics, including the scaling and structure of $P_{th}(n)$, by extending the 1D model. This study is motivated by recent experiments[26–28,36,37] which suggest aspects of the roles of electron and ion transport and heating in producing a power threshold minimum for LH transitions. In particular, the crucial role of the edge $(\nabla P_i/n)'$ in locking in the H-mode has been indicated and linked to the ion heat flux at the edge. All this must also be reconciled with the observed role of fluctuation power coupling to shear flows, which initiates the transition.[18] Thus, a focus of this work is on the missing link between *microscopic* turbulence physics and *macroscopic* dynamics, and on the role it plays in power threshold scaling. The major goal is to understand the physics which underpins the observed minimum in $P_{thr}(n)$. Based on our model study and comparison with experiments, we propose and examine the following interpretation of this phenomenon:

(i)   the ion heat channel is ultimately responsible for the transition as it builds up the diamagnetic electric field $\propto \nabla\langle P_i \rangle$ at the edge, required for the transition. However,

(ii)   the initial trend of a decrease in $P_{thr}(n)$ with increasing density is primarily associated with the dominance of electron heating over the ion heating in the low-density regime. This opens the door for shifting the heat from electrons to ions at higher densities. Such a shift progressively improves the conditions for LH transition, through the *cumulative* effect of the following two factors, both of which are crucial to produce the P_{thr} decrease:

   (a)   the increase in *collisional* heat transfer from electrons to ions.

   (b)   the increase of the heat *fraction* coupled to ions independent of the *collisional* electron-to-ion heat transfer.

(iii) the subsequent increase in $P_{thr}(n)$ is due to the increase in damping of turbulence driven shear flows with ion collisionality (that also grows with density). This scaling reveals the turbulence-generated shear flow as a trigger mechanism, as was indicated by the preceding studies.[10]

Neither (a) nor (b) in (ii) suffices to reverse the trend of increasing P_{thr} with density caused by the increasing shear flow damping which prevails in (iii). Only in the low-density regime do they work together, so the minimum in the $P_{thr}(n)$ curve can be interpreted as the crossover point between the trends (ii) and (iii). However, the recent ASDEX results[27] indicate that even for pure ECH, the $P_{thr}(n)$ decreases with n in the low-density regime. This result apparently eliminates our requirement (ii.b) above. We reconcile it with our model predictions by speculating that some part of the ECH energy is transferred to ions by collisionless mechanisms—either via heating or via anomalous coupling (turbulence)—which would be equivalent to (ii.b) and bypass (ii.a) above. We briefly discuss this possibility in Sec. V.

To address the premises (i)–(iii), the model must evolve electron *and* ion temperatures separately. The previous model[10] is based on a single fluid approach and does not separate species, nor does it allow for primarily ion (ITG) or electron (CTEM) mechanisms. Therefore, we extend it in the directions outlined below, so as to study the physics of the power threshold minimum. In the new model, apart from the separate equations for electron and ion heat transport, an electron-ion coupling parameter enters as well as the ZF shear damping, $\propto T_i^{-3/2}$. The important effect of collisional electron-ion coupling is retained, and separate ion and electron heat sources allow consideration of an arbitrary heating mix. Thus, we can in principle separate coupling effects from heating mix effects. This is usually not possible in experiments. As the electron heat transport is now treated independently, it is logical to include trapped electron modes in the turbulence field. This allows us to investigate the relation between the $P_{th}(n)$ minimum, and the location of Ohmic saturation in the $s_E(n)$ curve.

The plasma density often varies, not only by itself but also in response to changes in other parameters, and so it is not so clear which of the changing quantities is crucial to the L-H transition. In many experiments, the heating mix (NBI-ECRH) varies along with the density. In recent ASDEX Upgrade studies, the low-density $P_{thr}(n)$ branch appears in ECRH plasmas.[27,28,36] In contrast, in recent JET experiments, electrons and ions are heated in approximately equal proportions.[26] It follows that understanding the minimum of the power threshold requires scans in more than one direction in parameter space. Based on the above considerations, in this paper we perform such scans in density and the ion/electron heating mix. The roles of the ion/electron heat deposition profiles and fueling depths in L-H transitions will be addressed in a separate publication.

The remainder of the paper is organized as follows. In Sec. II, we briefly review the model and present its new features. In Sec. III, we describe our methodology to detect and document the L-H transitions. We present the results of the model in Sec. IV, followed by a Discussion section that lists the principal results, addresses remaining uncertainties, and discusses next steps.

II. THE 6-FIELD MODEL

Proceeding from the 5-field, 1D model described in detail in Ref. 10, we add a heat transport equation for

electrons. An electron-ion heat exchange term is also added to the respective ion equation. These two equations can be written in terms of the electron and ion pressures as follows:

$$\frac{\partial P_{i,e}}{\partial t} + \frac{1}{r}\frac{\partial}{\partial r}r\mathsf{C}_{i,e}^{(p)} = 6\frac{2m}{Ms_e}(P_e - P_i)$$
$$+ Q_{i,e}\exp\left[\frac{(r - a_{i,e})^2}{2\mathrm{D}r_{i,e}^2}\right], \quad (1)$$

where $s_e \propto T_e^{3/2}/n$ is the electron-electron collision time, m/M is the mass ratio, $Q_{i,e}$, $a_{i,e}$, and $\mathrm{D}r_{i,e}$ are the electron and ion heating rates, heat deposition locations, and heat deposition widths, respectively. The fluxes $\mathsf{C}_{i,e}^{(p)}$ are introduced in the same way as in Ref. 10. Here, $\mathsf{C}_i^{(p)} = -(\mathrm{v}_{\mathrm{n.t.}} + \mathrm{v}_0)\partial P_i/\partial r$ where $\mathrm{v}_{\mathrm{n.t.}}$ denotes the non-turbulent part of the ion heat transport, while its turbulent part is

$$\mathrm{v}_0 = \frac{s_c c_s^2 I}{1 + a_t\langle V_E\rangle'^2}. \quad (2)$$

The neoclassical contribution to the electron heat transport across the magnetic field is feeble compared to that of the ions (a reduction factor $0.02 \sim \sqrt{m/M}$), due to the small electron Larmor radius. The situation with the turbulent transport is more complicated, so for simplicity, we assume here the same transport for electrons. This will be improved in the next version of the model. The remaining notation that we use here is standard and explained in Ref. 10. The main quantity that drives the particle transport is the DW intensity I. It is governed by the following equation

$$\frac{\partial I}{\partial t} = \left(c_L - \mathrm{D}\mathsf{x}\,I - a_0 E_0 - a_V\langle V_E\rangle'^2\right)I + \frac{\partial}{\partial r}\mathrm{v}_N I\frac{\partial I}{\partial r}. \quad (3)$$

As in the previous model, the terms in the parentheses control the growth and decay of the DW intensity. They have the following meanings (from left to right): linear growth rate, nonlinear saturation, damping due to the ZF and MF shears, respectively. The last term on the r.h.s. describes the radial diffusive self-spreading of the DW intensity. The instability growth rate c_L in Eq. (3) is given by

$$c_L = c_{0i}\frac{c_s}{R}\left[\frac{R}{L_p} - \frac{R}{L_n} - \left(\frac{R}{L_{T_i}}\right)_{crit}\right] + c_{0e}c_s\left[\mathrm{r}L_{T_e}^{-1} + L_n^{-1}\right]. \quad (4)$$

The first term on the r.h.s. of this equation is identical to that used in Ref. 10 for the ITG drive with the threshold term $(R/L_{T_i})_{\mathrm{crit}}$, while the second term is new; it corresponds to the TEM contribution to the growth rate of the DW (with a numerical factor $\mathrm{r} \sim 1$). However, in our simplified model, these two different instability mechanisms both pump energy into the DW spectrum, characterized by the single intensity I. As the TEM part of the growth rate is composed of the temperature and density gradients additively, with a significantly softer threshold than the ITG flux dependence near the onset of instability, we neglected the TEM threshold in the above formula.

The remaining three equations are equivalent to those used in Ref. 10 in form, but the ion-ion collision frequency in these equations is now evolved through the local temperature and density. The same is not true for Eq. (1), which contains the fixed collision time for electrons. Both collisional and anomalous particle transport coefficients are thus also evolved and are coupled to the particle source. The collisional diffusivity is much smaller than the turbulent diffusivity, $D_{\mathrm{n.t.}} \ll D_0$ (see equations below). The particle transport, with deposition at the rate C_a, is governed by the following equation which is valid both for electrons and ions by virtue of quasineutrality

$$\frac{\partial n}{\partial t} + \frac{1}{r}\frac{\partial}{\partial r}r\mathsf{C}^{(n)} = \mathsf{C}_a\frac{a - r}{L_{dep}^2}\exp\left[\frac{(a - r)^2}{2L_{dep}^2}\right]. \quad (5)$$

Here, the flux

$$\mathsf{C}^{(n)} = -(D_{\mathrm{n.t.}} + D_0)\frac{\partial n}{\partial r} + V_n n$$

includes along with the diffusive part discussed above, the density pinch term with velocity[38]

$$V_n = -V_{n0}(D_{\mathrm{n.t.}} + D_0)(2/R + 1/L_T).$$

$D_0 = \mathrm{v}_{0,e}$ is assumed throughout this paper. Next, the poloidal mass flow velocity is evolved according to the following equation:

$$\frac{\partial\langle V_\vartheta\rangle}{\partial t} = -a_5 c_{0i}c_s^2\frac{a}{R}\left[\frac{R}{L_p} - \frac{R}{L_n} - \left(\frac{R}{L}\right)_{crit}\frac{\partial I}{\partial r}\right]$$
$$-\mathsf{l}^{neo}\nu_{ii}q^2 R^2\left(\langle V_\vartheta\rangle - 1.17 c_s q_i L_T^{-1}\right).$$

The numerical factor 1.17 is strictly valid for large aspect ratio tokamaks in banana regime[39] and may become inaccurate at the edge. The role of this term, however is not important for this model,[10] so we use this form, for simplicity. The poloidal velocity will be used to obtain the mean flow shear below which in turn is needed to calculate the transport coefficients v_0 and D_0

$$\langle V_E\rangle' = q_i c_s L_p^{-1}(L_p^{-1} - L_n^{-1}) - \langle V_\vartheta\rangle'. \quad (6)$$

Finally, the equation for the ZF energy has the following form:

$$\frac{\partial E_0}{\partial t} = \frac{a_0 E_0 I}{1 + f_0\langle V_E\rangle'^2} - c_{\mathrm{damp}}E_0.$$

The numerator of the first term describes the DW drive of the ZF, while the denominator accounts for the mean flow shear suppression of the ZF growth. The second term corresponds to the collisional damping of the ZF. Again, all the parameters and constants not noted explicitly above are the same as in Ref. 10, except ν_{ii} and $c_{\mathrm{damp}} \propto \nu_{ii}$ now depend on the local density and temperature rather than on the respective reference values.

III. IDENTIFYING AND DOCUMENTING L fi H TRANSITIONS

Introducing a new feedback loop into the L → H transition model—such as the (electron) heating channel with ion coupling, along with the dependence of this coupling on the local density and temperatures—makes some of the transitions appear different from those seen on the previous model, depending on the transition regime. The main issue in identifying the transition is that the variations of physical quantities at the transition point are very small in certain regimes, particularly when the density is low. It is not always possible to distinguish these variations from the conventional time variability of the system. Moreover, there are documented cases (as we will see when discussing Fig. 4 below, lower left surface plot) in which a seemingly well established low-n pedestal with markedly enhanced ∇P_e does not survive and the system returns to the L-state. This particular example arises in the low-density regime with pure electron heating.

Therefore, before discussing the dependence of the L → H transition power threshold P_{thr} on the plasma density and other variables, we first describe the transition criteria for this model. Using these criteria, in each run we will determine: (i) if a transition occurred and if yes, (ii) what values are to be ascribed to the relevant variables at the transition point. Apart from the clear-cut cases illustrated below, many transition candidates require an inspection of more than one quantity to distinguish them from general time variability of the system. From the menu of "official" H-mode criteria, which include a drop in H_a/D_a signals and the formation of a pedestal in the density profile, we can (obviously) use only the latter in this study. To make matters more difficult, the temporal growth in *spatially averaged density* associated with the buildup of the pedestal at the *edge,* is often too slow to resolve the transition in time, and even to determine whether or not it occurred at all. Otherwise, the *spatially averaged* quantities are more practically useful transition indicators than the physically more meaningful density gradient at the *edge*. In particular, the transition identification problem occurs in low-density regimes, where the edge gradients typically develop slowly and cannot be readily identified. At the same time, spatially averaged ZF, MF, and DW typically vary more noticeably in time. For example, DW intensity drops strongly at the transition so, we use these variations as the transition signature instead of the density jump, when the latter is too small to measure (examples will be given and discussed below, Fig. 2).

However helpful the average quantities, an inspection of the *spatio-temporal* behavior of the transition is required for its identification, primarily via the buildup of edge gradients. The incidence of a strong MF jet, narrowly peaked at the edge, is another transition signal. It is important to note that, as the neoclassical heat transport of electrons is strongly suppressed in the current model, ∇P_e is stronger at the edge than ∇P_i and even ∇n during and after the LH transition (cf. Ref. 27). Turning to the quantitative criteria of L → H transitions that we applied in this study, they are somewhat different in the cases with and without the preceding limit-cycle oscillations (LCO). For the former, we require that the

variation in at least one variable is double the oscillation amplitude or more and the transition occurs in a period of time shorter than the LCO period. In the non-LCO cases, we require that at least one of the variables changes by at least 20%. The other variables may show only feeble signs of transition, which is exemplified in Fig. 2. Before considering marginal, low-density transitions described above, it is worthwhile to start from a clear-cut transition, as shown in Fig. 1. Here, four quantities (core line-averaged plasma density, ZF, MF, and DW), all of which clearly change at the transition, are plotted as functions of the heating rate $Q(t) = Q_i + Q_e$, rather than the more commonly used time. Since we use a non-decreasing $Q(t)$ source, this representation of the transition dynamics has the advantage of yielding the value of the power threshold $P_{thr} \equiv Q(t_{trans})$ directly. In other words, we do not need to obtain the t_{trans} first and then determine P_{thr} by matching it to the $Q(t)$ curve. Note that the temporal variation of $Q(t)$ can still be extracted from the density of the data points on each curve in Figs. 1 and 2, which are given at equal time intervals. The core line-averaged density is chosen as an "independent" variable in $P_{thr}(n)$ instead of the edge density, because it is used in many experiments and because it is a robust characteristic of $e - i$ thermal coupling, crucial to the transition. Indeed, as electron heat is deposited in the core, its coupling to the edge temperature and density gradients depends strongly on the density and temperature in the core. This embodies the interplay between the macroscopic core transport phenomena and mesoscale edge phenomena in L-H transition dynamics.

For the purposes of the present study, where we do not consider back transitions and hysteresis, the most effective choice of the time dependence of heating power appears to be the following. We nominally divide each run into three phases. During the initial phase, $Q(t)$ is kept at a reasonably low level, chosen so as to maintain the L-mode. If Q was fixed at this level, the system would reside in the L-state indefinitely long. To initiate transition, we gradually raise Q in the second phase. It is this phase during which the L → H transition is expected. If it occurs, the purpose of the third phase is to make sure that the established H-mode is sustainable. In that regard, this phase is similar to the first one, as Q is kept nearly constant, though at an elevated level.

More specifically, the heating rate $Q(t)$ varies with time between its initial value $Q_{min} = Q - DQ/2$ and final value $Q_{max} = Q + DQ/2$ as follows $Q = Q + DQ\tanh(t/Dt)/2$. As explained above, the macroscopic heating ramp time Dt is deliberately chosen to be much longer than the characteristic (microscopic) transition time but significantly shorter than the duration of the initial and final phases, during which Q stays close to its respective initial and final values. This separation of the time scale enforces spontaneous transitions which occur between two quasi-stationary states of the system, so as to separate them from variations caused by the time dependence of $Q(t)$. Of course, there are limitations to this statement—we must choose DQ and Dt appropriately, for practical reasons. But this particular choice of power ramp has proven efficient in scanning extended domains in parameter space. In most cases, it produces a transition in a
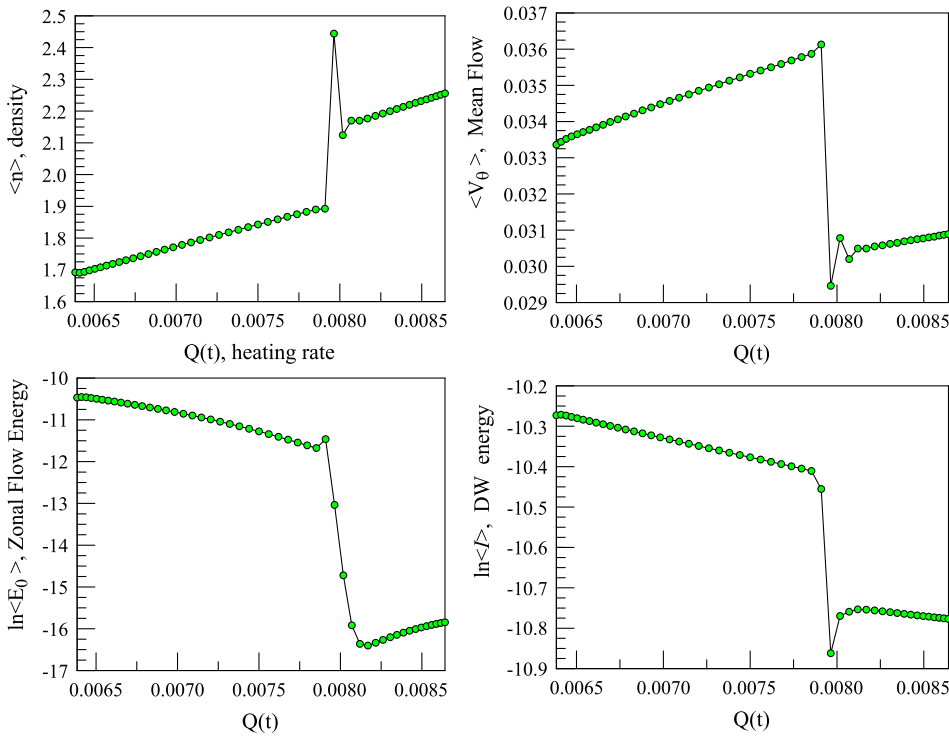
FIG. 1. L → H transition event shown in four characteristic variables, core line-averaged: density, ZF energy, MF $E \times B$ velocity, and DW energy. They are shown as functions of the heating rate $Q(t)$ rather than time t, where Q varies between Q_1 and $Q_2 > Q_1$ indicated as the beginning and the end of the integration interval. Here, $dQ/dt > 0$ over the integration time $t_1 < t < t_2$. Data points are taken at equal time intervals, so their density on each curve indicates both the rate at which Q is changing and how quickly the changes in the variables occur.

single run. If not, we continue it by adding another DQ-increment to the maximum Q, reached before.

Again, in the low-density regimes the density jump Dn across the transition often becomes indistinguishable from the common system variability, while the jumps in other quantities (such as ∇P_e at the edge) remain clearly identifiable. We use these quantities to register transitions in such cases. Examples are shown in Figs. 2 and 3.

Finally, to validate a transition we make sure that there is no back transition in the absence of a decrease in power or

change in fueling. These transient phenomena (or failed transitions) occur in runs executed for system parameters typical for the weak transitions at low density, as mentioned earlier. A surface plot representation of the spatio-temporal evolution of the system is most useful for this purpose. First, we give a clear-cut example of a strong transition preceded by an I-phase, shown on the top row of Fig. 4. A strong mean $E \times B$ flow shear jet localized at the edge is one clear signature of an established H-mode. This is illustrated in Fig. 5, along with the spatial distributions of other important
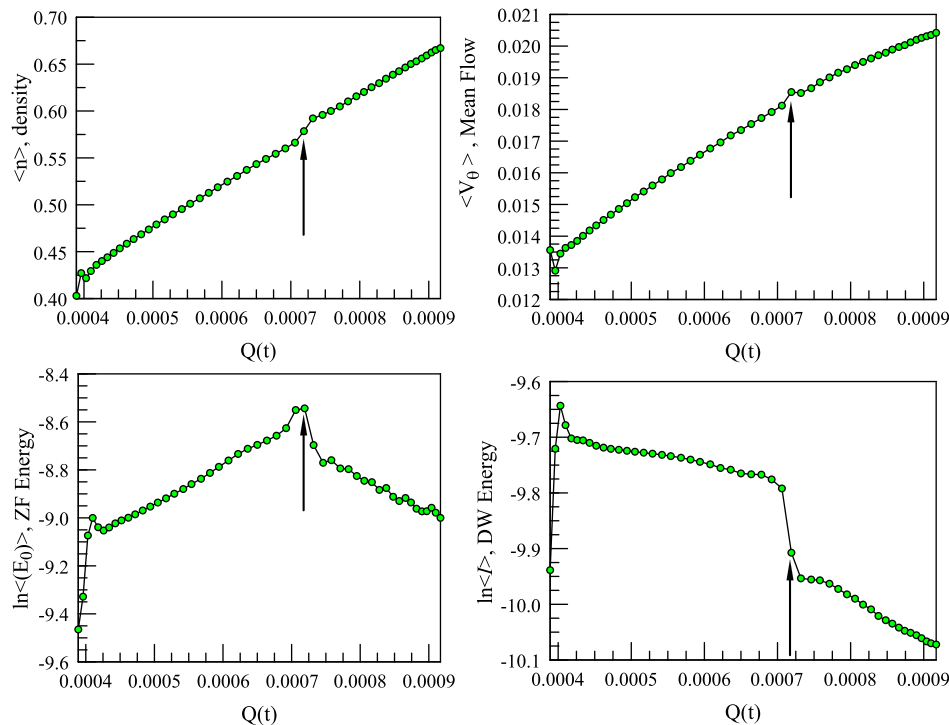

FIG. 2. The same as in Fig. 1 but for the case of a weak transition. Arrows show the time which is considered to be the LH transition point. Rapid changes of dependent variables at the beginning of integration show a fast relaxation to the L-mode (effect of initial conditions).
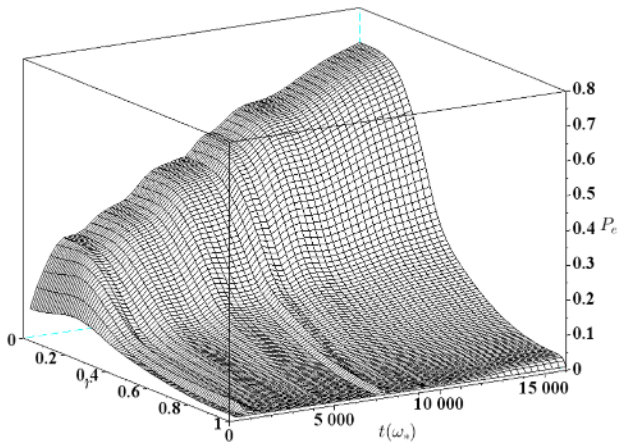
FIG. 3. Example of weak LH transition shown in terms of electron pressure P_e as a function of time and radius. Unlike the case shown in Fig. 4, the pedestal gradually builds up only after the actual transition occurs at $t = 10\,000$.

FIG. 5. Radial distributions of DW, ZF, and MF for $H_{\mathrm{mix}} = 0.7$.

ingredients of the L → H transition, the DW and ZF. This particular case is one of a strong H-mode. It will also be used in the discussions of physical characteristics of strong H-mode states later in the paper.

Note that the ZF energy drops but does not vanish completely, even after a strong transition, unlike in the 0D model.[3] The same is true for the DW energy (not shown in Fig. 4). These observations help us to identify and reject failed transitions, such as that shown on the bottom row of Fig. 4. Namely, an H-mode state appears here in the middle of the ramp-up phase and, indeed, a mean flow jet forms near the edge, signifying the transition. However, the jet is not well isolated from the MF in the core so, they merge into
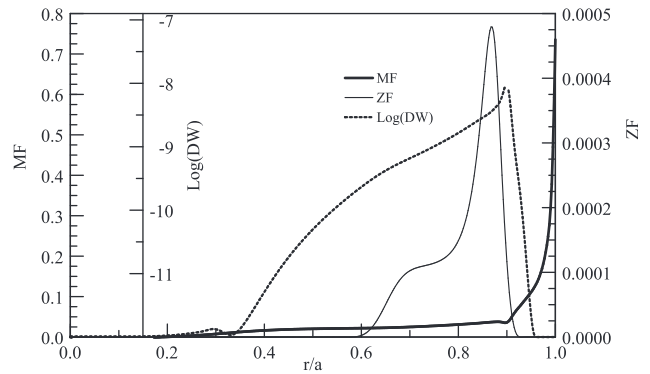
a smooth, large scale MF which does not provide sufficient shear to suppress turbulence and transport. This leads to a back-transition, even though the power is still rising. We reject these events as LH transition candidates.

When an LH transition is validated using the rules described above, we still need to assign specific values to relevant quantities at the moment of transition. The most natural choice would be to use the quantities *immediately* preceding the transition. The difficulty with this choice occurs when the system undergoes a transition through an I-phase (e.g., Fig. 4, upper row). The relevant quantities oscillate quite strongly prior to the transition, thus making the pre-transition value ambiguous. In this case, it is important to distinguish among: (a) values at the beginning of the I-phase, (b) time-averaged values during the I-phases, and (c) values just prior to I → H transition. The same is true for the post transition values, particularly because of significant
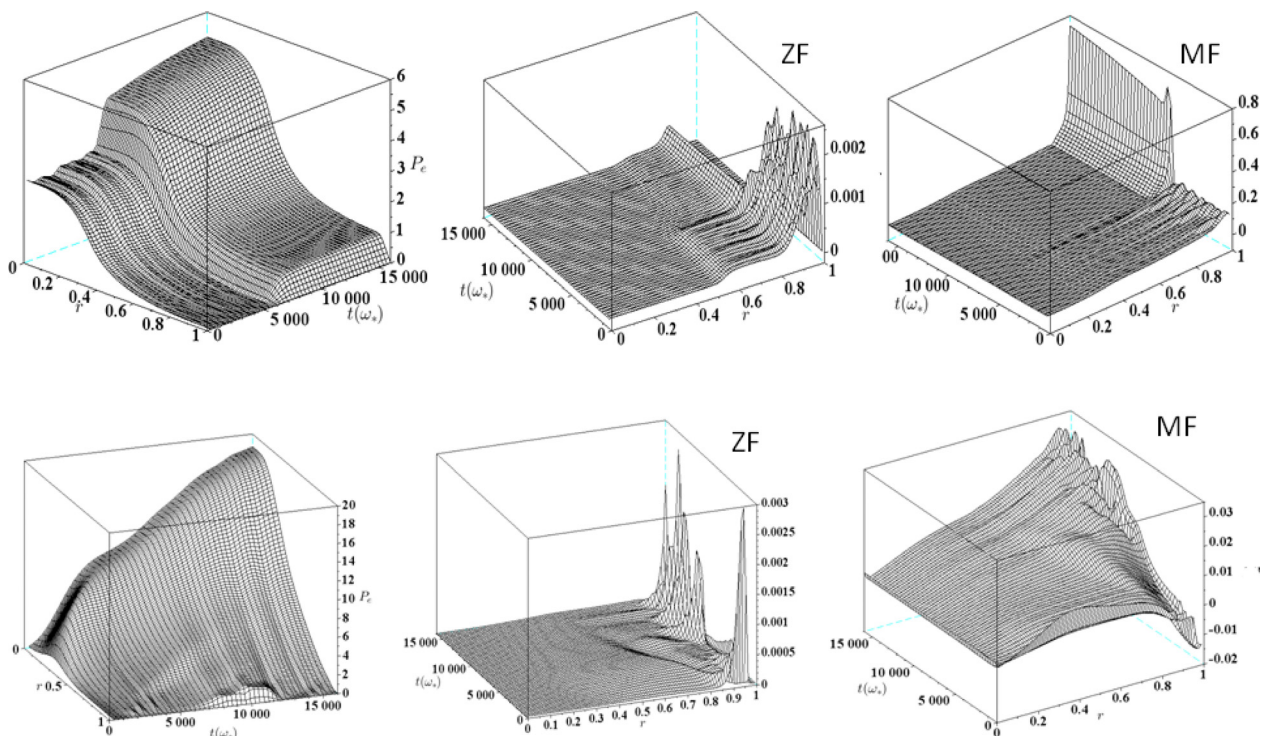

FIG. 4. Top row: an example of LH transition with an extended pre-transition I-phase, shown for the electron pressure P_e, ZF energy and the MF velocity. Strong, edge-localized MF is a marker of the H-mode. Bottom row: an example of a failed transition with inward propagation. The edge MF jet starts to form but then merge with the large scale MF.

overshoot and the ensuing oscillations. Therefore, to register the transition point for a quantity that, say, grows in time during the transition, we use its value midway between the last minimum *before,* and the first maximum *after,* the transition. An example of this procedure is shown with the arrows in Fig. 2.

IV. RESULTS

With the above method for documenting the transition, *we proceed to investigate possible mechanisms for the observed minimum in the power threshold* P_{thr} (*n*), where *n* is the core line-averaged density at the moment of LH transition. Focusing on this goal, we will scan P_{thr} in reference density (n_{ref}), and ion/electron heating ratio, as we can directly control these parameters, unlike *n*. Since we have added new components to the model, it is necessary to begin by making contact with its previous versions. The respective model studies were made by scanning the reference density n_{ref} (in ZF damping rate $c_{damp} \propto n_{ref}/T_{ref}^{3/2}$) measured in the previous model[10] in the units of 10^{20}m^{-3}, which has been adopted in this paper. Note that n_{ref} is fixed during each LH transition. The monotonic growth of $P_{th}(n_{ref})$ was thus caused by the growth of ZF damping, as it requires more power to trigger the transition. By contrast, in the new model the ZF damping depends on the density and temperature ($c_{damp} \propto n/T_i^{3/2}$) *which evolve in time* and *space,* so the simple monotonic dependence is not guaranteed, on account of these new feedback loops. Also, as we already remarked, n_{ref} is used here as a control parameter to generate the dependence P_{thr} (*n*). *The latter is thus not a scan of* P_{thr} *in n but rather a parametric representation of two functions,* $P_{thr}(n_{ref})$ *and* $n(n_{ref})$ *in the* (*n*, P_{thr}) *plane. This will be shown as a scatter plot in Fig.* 6 *below.* Of course, *n* depends not only on n_{ref} but also on other parameters, such as the fueling rate c_a (Eq. (5)), density at the boundary (both scaled to n_{ref}), parameters in the transport coefficients, etc. (kept fixed at levels inherited from Ref. 10). To probe the power threshold P_{thr} (*n*), we will change only n_{ref} or H_{mix} from run to run.
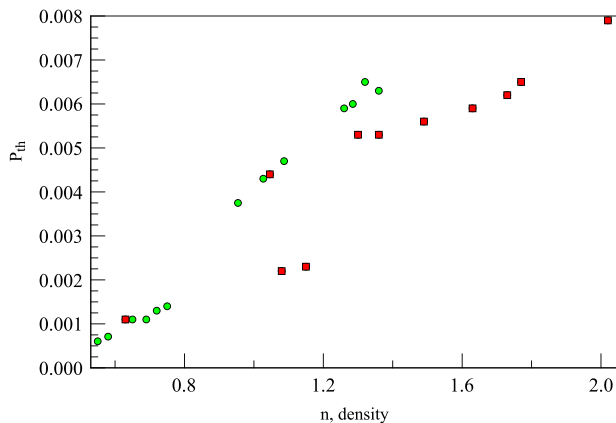

FIG. 6. Scatter plot of the power threshold for the LH transition P_{thr} shown against the core line-averaged density. Squares indicate strong transitions with the density jumps   0.1 or stronger. Circles indicate weaker transitions. Throughout this paper, we use equal values for the widths of the heat sources $Dr_e = D\, r_i = 0.15a$, for electrons and ions, (see Eq. (1)), and for the heat deposition radii $a_{e,i} = 0.3a$.
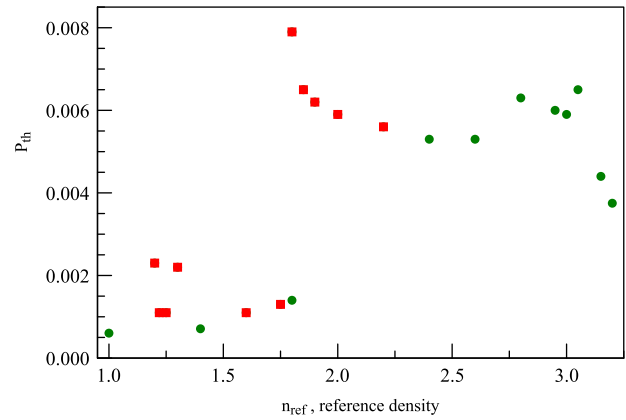

FIG. 7. The same as in Fig. 6 but as a function of reference density, n_{ref}.

The above choice of the density variable *n* is suggested by our results below, as the data are better organized in *n* than in n_{ref}. More importantly, this choice of *n* is consistent with most of the experiments. To justify this choice and to see the effect of the new feed-back loops, we present the P_{thr} as two separate functions P_{thr} (*n*) and $P_{thr}(n_{ref})$ in Figs. 6 and 7. As we discussed, *n* is *not a control parameter* of the model and is related to the control parameter n_{ref} only in a rather complicated way. This point is illustrated in Fig. 8 generated from the same data set as the Figs. 6 and 7. Clearly, *n* is related to n_{ref} depending on the regime of any given LH transition. In particular, transitions at rather close values of n_{ref} vary abruptly in their strength (e.g., jump in *n*) and in other aspects, such as the presence of an LCO. Currently, we do not have a simple physical explanation for the $n(n_{ref})$ dependence shown in Fig. 8 but, as it embodies a distinct bifurcation phenomenon, sharp variations of the order parameter at points that may be considered as critical should not be surprising.

In these runs the external heat is deposited into the ions, which corresponds to the previous model studies. The electrons heat only by collisional heat exchange with ions. Strong transitions with the density variation $Dn > 0.1$ are marked out with the squares. Fig. 6 shows that the general trend is an increase of P_{thr} with *n*. This is largely consistent with the results of the preceding model,[10] given the
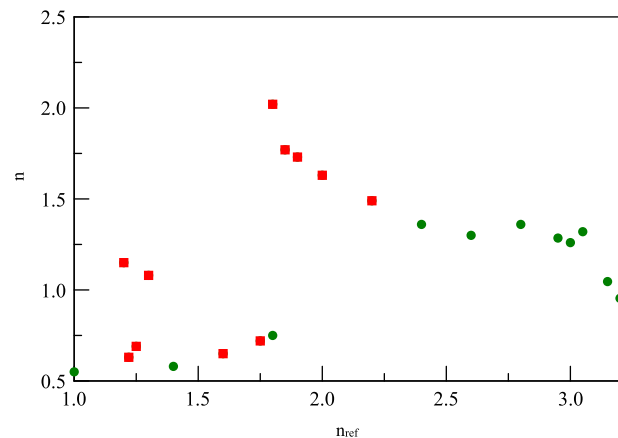

FIG. 8. The core line-averaged density *n* as a function of reference density n_{ref}, shown using the same data set as in Figs. 6 and 7.

reservations regarding the choice of n vs n_{ref}, discussed above. There is a noticeable difference from the previous model results in the low-density regime, which can be attributed to the dependence of the ZF damping on the local plasma density and temperature in the new model. In particular, there are regions of a non-monotonic $P_{thr}(n_{ref})$, clearly resulting from non-monotonic relation between n and n_{ref}, Fig. 8. These data are also indicative of possibly non-single-valued $P_{thr}(n)$, as shown in Fig. 6. Such behavior is not surprising as those plots are merely the projections on the (P_{thr}, n)-plane of a presumably more complicated functional relation between these variables in an extended parameter space. These relations more fully describe the transport bifurcation and they include new feedback loops, absent in the previous model.

It might be tempting to relate the local minima in $P_{thr}(n_{ref})$ produced by the new model and shown in Fig. 7, to those observed in the experiments, e.g., Ref. 28. However, the experimental minima are broader by a factor of two or more, and noticeably deeper. The model-produced $P_{th}(n_{ref})$ also shows a quasi-discontinuous behavior in the low-density regime, as discussed in the previous paragraph. Although the experimental data are scattered, there is no clear indication of such a feature in them. More importantly, we need to use the core line-averaged n instead of n_{ref}, to compare model predictions with experiments, as discussed earlier.

So, we turn to the premise put forward in the Introduction and test whether the minimum in $P_{thr}(n)$ results from $e-i$ thermal coupling acting together with the ZF damping, by studying the response of *both* these quantities to n. First, we explore the $P_{thr}(n)$, when all the heat initially goes to electrons, while ions receive it from them only via collisions. The results are presented in Fig. 9 and they show a smooth monotonic growth of the power threshold with density. The obvious difference from the pure ion-heating case, discussed above, may be attributed to a mediated heat transfer to the ions, but the general trend of growing power is consistent with the idea that the ions are the key for the transition and the ZF damping increase is the cause for $P_{thr}(n)$ to increase with density. We note here that this behavior is on the surface inconsistent with one recent experiment[27] which claims a monotonic decrease of P_{thr} with n for a pure ECH
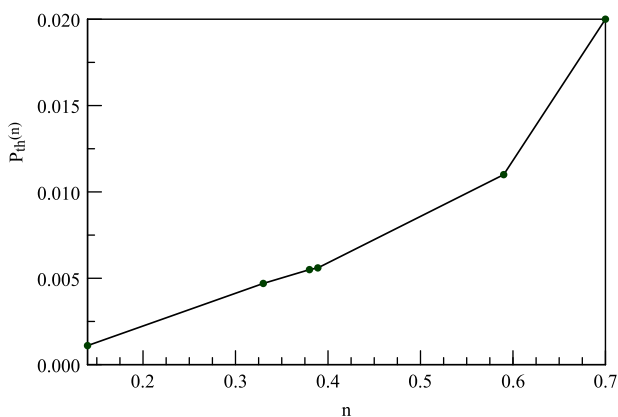
regime. We will discuss this issue below, and proceed now with the original plan.

As there is no clear minimum in both pure electron and pure ion heating regimes, we attempt mixed heating. For this purpose, we introduce a control parameter that characterizes the mix of ion and electron heating in Eq. (1) as follows:

$$H_{mix} = \frac{Q_i}{Q_i + Q_e} \equiv \frac{Q_i}{Q}. \qquad (7)$$

This definition obviously implies that $Q_i = H_{mix}Q$ and $Q_e = (1 - H_{mix})Q$, where Q denotes the total power deposited into the plasma. We will vary H_{mix} between 0 and 1. The above results shown in Figs. 6–8 and Fig. 9 correspond to $H_{mix} = 1$ and $H_{mix} = 0$, respectively. In a general case of $0 < H_{mix} < 1$, this parameter characterizes the local partition of the heating power between the two species. We exploit H_{mix} to isolate the effects of thermal coupling between the species on the LH transition. As the experiment[28] suggests, at the low-density end of the P_{thr} data, the power goes mostly to electrons (i.e., as for ECH) implying $H_{mix} \ll 1$; at the high density end it goes to ions as if for NBI, that is $H_{mix} \approx 1$. The most recent ASDEX experiment,[27] though, made it possible to apply the ECH throughout the low-density branch of the $P_{thr}(n)$ curve. Nonetheless, it is not obvious that this situation truly corresponds to the choice $H_{mix} = 0$ in our model, Fig. 9. The reason is that a significant part of the electron heat may be transferred to the ions anomalously by collisionless processes – an effect which is not included in the heat exchange in Eq. (1). This would correspond to $H_{mix} > 0$ in the model, even if only ECH is applied. Simply put, H_{mix} is a control parameter of the model but we cannot map it to heat partition in the real experiments quantitatively, because we do not know the fraction of the electron heat that possibly bypasses Eq. (1) on its way to the ions. We will discuss this problem somewhat further in Sec. V.

Under these circumstances, our strategy is to obtain the dependence of $P_{thr}(n, H_{mix})$, first on both n and H_{mix} as on independent variables. Then, by imposing a plausible constraint on these variables as $H_{mix} = H_{mix}(n)$, we reduce $P_{thr}(n, H_{mix})$ to a function of a *single* variable n, that is $P_{thr}(n) = P_{thr}[n, H_{mix}(n)]$. This function can be directly compared against the P_{thr} profile obtained experimentally. To implement this plan we have performed a scan sampling $200 +$ transition candidates. Note that the methodology outlined in Sec. III allows us to do this efficiently. Some 60 transitions have been selected and are presented in a form of a 3D scatter plot of the function $P_{thr}(n, H_{mix})$ shown in Fig. 10. *These results demonstrate that once the heating mix changes in the way we described—that is H_{mix} grows monotonically with n for the data set presented in Fig. 10—the power threshold must pass through a minimum.* Indeed, based on experimental settings,[28] the $H_{mix}(n)$ constraint on the (n, H_{mix}) plane, should connect the corner for $H_{mix} \simeq 1$ and high n, with the opposite corner $H_{mix} \simeq 0$ and low n. We see that unless the density at the end of this path is taken to be extremely low (where, at best, only marginal transitions occur) a minimum in $P_{th}(n, H_{mix})$ cannot be missed. While its exact shape depends on the specific choice of the $H_{mix}(n)$
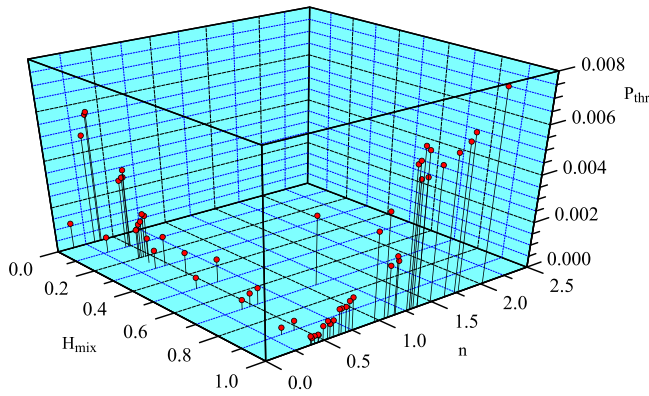
FIG. 9. The same as Fig. 6 but with $Q_i = 0$, Eq. (1), that is the heat here is deposited into electrons.

FIG. 10. 3D scatter plot of transition power threshold P_{thr} in heating mix - density variables, H_{mix} and n. The choice of n, H_{mix} points in the sample is dictated by the experimental trend of electron biased heating at lower densities and ion biased heating at higher densities. However, an extended subsample at $H_{mix} = 1$ (pure ion heating) is also included into the plot.

constraint—which should be provided by the experiment—we see that the *minimum is generic*.

It must be noted that the coverage of the (H_{mix}, n) plane could be better even though the model efficiency in selecting and classifying the transitions is greatly improved as compared to the earlier versions. The choice of (n, H_{mix})- sample shown in Fig. 10 is dictated by the experimental trend of electron biased heating at lower densities and ion biased heating at higher densities. However, an abundant subsample at $H_{mix} = 1$ (pure ion heating) is also included into the plot. As we emphasized earlier, n cannot be varied at will, which partially explains the limited coverage. Nevertheless, it is easy to see that if we navigate through the data set from the high n, $H_{\text{mix}} = 1$ corner to moderately low n, $H_{\text{mix}} = 0$ corner, the value of P_{thr} will pass through a minimum.

To illustrate this aspect of the results, we select a subset of data points from the sample in Fig. 10. The subset is constrained by merely the condition of monotonic growth of $H_{mix}(n)$, but is otherwise arbitrary. The resulting dependence of $P_{\text{thr}}(n)$ is shown in Fig. 11. We also plot the $H_{mix}(n)$ constraint, adopted to generate the $P_{\text{thr}}(n)$ profile. It is important to emphasize here that, given the absence of clear minima in $P_{\text{thr}}(n)$ or $P_{\text{thr}}(n)$ shown in Figs. 6 and 7, the minimum in
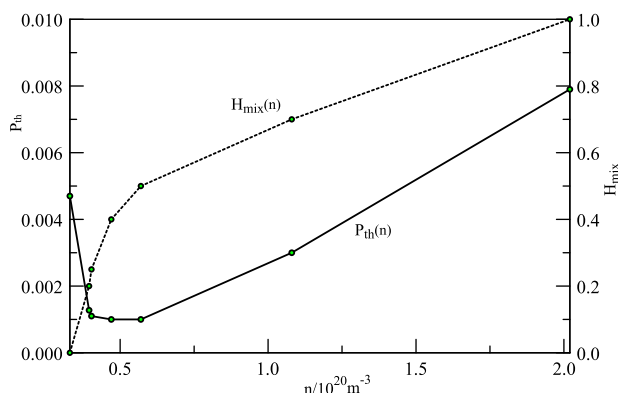

FIG. 11. Dashed line: monotonic dependence of $H_{mix}(n)$, arbitrarily chosen from the sample shown in Fig. 10. Solid line: the resulting $P_{\text{thr}}(n)$, constrained by the relation shown with the dashed line.

$P_{\text{thr}}(n)$ in Fig. 11 largely results from the hidden $H_{\text{mix}}(n)$ dependence in the function of two variables $P_{\text{thr}}(n, H_{\text{mix}})$, as explained in the preceding paragraph. We discuss the physical ambiguity in $H_{mix}(n)$ selection in Sec. V.

V. DISCUSSION AND CONCLUSIONS

The primary objective of this work has been to elucidate the physics of the minimum in the L $\rightarrow$ H power threshold as a function of plasma density, n. The principal results of our investigation are:

(i)   LH transitions are initiated when the ion pressure gradient at the edge becomes strong enough to generate strong zonal flow and mean flow shear.

(ii)   Before locking in to the H-mode, these quantities typically fluctuate, with some trend of inward propagation, over a broad region adjacent to the edge.

(iii)   The subsequent lock in to a strong H-mode is characterized by the following processes, occurring nearly simultaneously:

   (a)   abrupt reduction of the spatially averaged intensity of the turbulence and fluctuation-driven flow components.

   (b)   build up of a strong laminar mean flow jet, narrowly localized at the edge.

   (c)   significant reduction and shift of the zonal flow shear peak inwards relative to the mean flow jet.

   (d)   build up of a strong gradient of ion and electron pressure at the edge, co-located with the mean flow jet but outside the zonal flow peak.

(iv)   The LH transition power threshold grows monotonically with the core line-averaged density in both *pure ion* and *pure electron* heating regimes with some flattening in low-density regimes, but with no clear minima.

(v)   The descending low-density branch of the $P_{\text{thr}}(n)$ curve, followed by a distinct minimum, results from a combination of the growing efficiency of electron-to-ion collisional heat transfer, together with the growing fraction of heat deposited into ions.

(vi)   The upturn of $P_{\text{thr}}(n)$ starts when the ZF damping prevails over the trends in (v), thus requiring increasingly more power for the transition.

(vii)   The heating mix $H_{\text{mix}}(n)$ is essential for the heat transport from the core to build up the ion pressure gradient at the edge, ∇P_i, which is the primary driver of the LH transition.

The data set on $P_{\text{thr}}(n)$, obtained in experiments, is rapidly expanding, e.g., Refs. 26–28, 36, and 40–42, but does not yet provide a direct relation between the $e - i$ heating ratio and the density, that is $H_{\text{mix}}(n)$ in our notation. As we saw, such a relation is crucial for the model calculations of the L-H power threshold $P_{\text{thr}}(n)$, and especially for its minimum. The comparison of the model predictions shown in Fig. 11 with the measurements shown in Fig. 3 of Ref. 28, for example, is nevertheless encouraging, as the model prediction is even quantitatively consistent with these results. However, the choice of H_{mix} here is somewhat arbitrary, albeit plausible, and not optimized to fit the data to the

model. Except for a rather special choice of the subset $H_{mix}(n)$ in Fig. 10, that would go into the corner of the lowermost n, $H_{mix} = 0$ from the high n, $H_{mix} = 1$ corner, the minimum in $P_{thr}(n)$ appears generic. Besides, it cannot be guaranteed that, depending on the choice of the subset, $H_{mix}(n)$ has no other local minima or maxima in the areas of the parameter space not covered by the study. However, based on the current data coverage, there is no evidence for that. It should also be noted that the precise shape of the $P_{thr}(n)$ curve depends on the subset choice and is constrained by the incomplete coverage of (n, H_{mix}) plane. All told, the prospects for extracting the $H_{mix}(n)$ curve from the observations merit a brief discussion.

In principle, the power deposited in electrons through ECRH can be measured accurately,[43] but requires dedicated experimentation to do so.[36] By including the NBI ion heating that dominates the high-density branch of $P_{thr}(n)$, one should be able to get an idea of $H_{mix}(n)$ dependence in real devices. However, other power sources may also contribute to P_{thr}. These include Ohmic heating and the power extracted from the diamagnetically stored energy.[26] In particular, Q_e in Eq. (7) should be taken as $Q_e = P_{ECH} + P_{Ohmic}$, while $Q_i = P_{ICRF} + P_{NBI}$, less the diamagnetic stored energy loss rate for ions. It appears then that the present day experiments should be able to condense their complicated heating schemes into the $H_{mix}(n)$ dependence, which is needed to test the model capability to reproduce the $P_{thr}(n)$ curve quantitatively. *The knowledge of the heating mix $H_{mix}(n)$ is essential to understand the energy pathway from the heat deposition $Q_{i,e}$ in the core to the ion pressure gradient at the edge, ∇P_i, which is the primary driver of the LH transition.*

Turning to the uncertainties and future improvements of the model, a sizable fraction of ECRH power can go to ions, thus compromising the assumed $H_{mix}(n)$ dependence through mechanisms not directly related to the collisional $e - i$ coupling.[44,45] For example, the ECRH/Ohmic-heated electrons may develop a suprathermal component (akin to runaway) which, in turn, can drive high frequency electron modes. This energy may collisionlessly couple to the ions, and is thus unaccounted for via the H_{mix} parameter. To give a simple example, the magnetized plasma waves $x \simeq x_{pe}k_{\parallel}/k$ $(x_{pe} < x_{ce})$, driven by anisotropic suprathermal electrons via the Doppler resonance $k_{\parallel}v_{\parallel} \simeq x_{ce}/c$, can redirect $\sim x/x_{ce}$ of their free energy to ions by nonlinear Landau damping,[46] rather than $e - i$ collisions. It follows then that along with understanding the link between the microscopic turbulent phenomena and the mesoscale flow shear due to the Reynolds work, we need to better understand the link between macroscopic energy deposition via core heating and the turbulence controlling ∇P_i at the edge.

For electrostatic turbulence, the explicit dependence of collisionless energy transfer on density can be expected to be weak. However, indirect dependence is possible, via the effect of zonal flow damping in regulating fluctuation intensity levels. Additional density dependence can enter through b, for electromagnetic turbulence.

In particular, note that this study suggests that the relation between the traditional experimental power control parameter (i.e., P_{thr}) and the physical quantity which actually controls the transition, namely, the edge ion heat flux $Q_i(a)$,

is not so simple, especially in electron heating regimes. The parameter $T = s_{equ}/s_{Ee}$ is relevant. Here s_{equ} is the collisional equilibration time and s_{Ee} is the electron energy confinement time. For $T > T_{crit} \sim \mathcal{O}(1)$, electron heat will be lost by transport before it can be coupled to the ions, resulting in a high P_{thr} – i.e., a large amount of power must be injected to achieve a sufficient $Q_i(a)$. For $T < T_{crit}$, sufficient electron heat is coupled to the ions to achieve an adequate $Q_i(a)$ at moderate power. This observation of a link between the collisional thermal equilibration and the minimum in $P_{thr}(n)$ is supported by Fig. 12 obtained from data from several tokamaks.[47] The figure shows the close relation between:

(a) The density at which the Ohmic energy confinement time saturates—i.e., rolls over from the linear Ohmic confinement (LOC) phase to the saturated Ohmic confinement (SOC) phase. This critical density is set by the competition between LOC electron thermal transport and collisional electron-ion coupling. This is effectively the content of the parameter T defined above. (N.B. Fig. 12 plots the critical density at fixed q, which implies fixed collisionality).

(b) The observed minimum in the $P_{thr}(n)$ curve. This close correspondence supports the hypothesis that the decreasing P_{thr} branch of the $P_{thr}(n)$ curve reflects an *increase* in $Q_i(a)$ due to increased collisional coupling of electrons heat to the ions.

Within the current model, we explored the L $\rightarrow$ H power threshold P_{thr} dependence on the core line-averaged density n, measured at the moment of transition. This was done by varying the $e - i$ heating ratio, H_{mix}, and the plasma reference

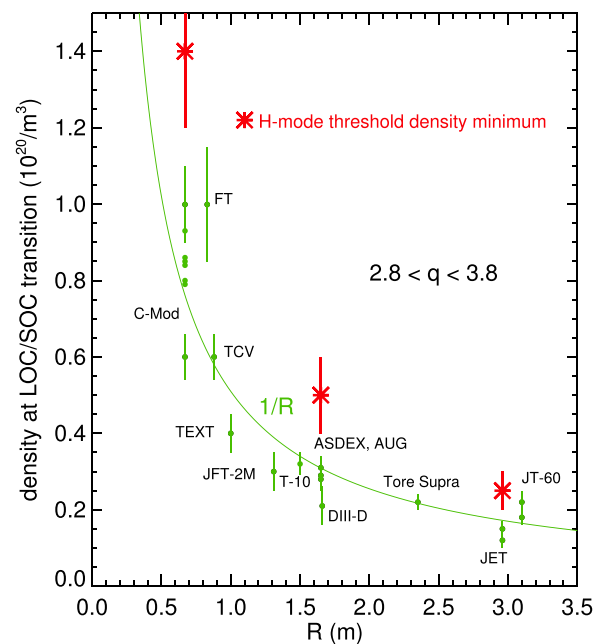

FIG. 12. Compilation of the data from several tokamaks showing the relation between the LOC/SOC transition density (smooth curve) and the $P_{thr}(n)$ density minima ("star" values). The correlation between the two trends is evident. Apart from the data points shown with the "stars," the plot is adopted from Fig. 7 of Ref. 47, where further explanations can also be found.

density n_{ref}. As we stated earlier, n is not strictly a control parameter in the $P_{\text{thr}}(n)$ dependence, while H_{mix} and n_{ref} are. But there are a number of other control parameters that may affect $P_{\text{thr}}(n)$. In order to understand the mechanism of the minimum in $P_{\text{thr}}(n)$ by varying the minimal number of control parameters that govern it, we kept the other control parameters fixed. These parameters are the fueling rate C_a and depth L_{dep}, [Eq. (5)], heat deposition radii $a_{e,i}$ and widths $Dr_{e,i}$ [Eq. (1)], as well as other model parameters whose influence on the system dynamics was examined using the preceding version of the model.[10] A preliminary assessment shows that the impact of the heat/particle deposition parameters on the L-H threshold is also strong enough to include them in the next study with this model. In particular, the impact of fueling other than by gas feed (i.e., pellets, SMBI, etc.) should be explored, as well.[34,48]

Our study indicates that, on the descending branch of $P_{\text{thr}}(n)$, ions must receive an increasingly higher fraction of the total heat available, in addition to the collisional heat input from electrons. On the high-density branch, where ions are heated (mainly) directly, and as the ZF damping grows with n, P_{thr} must also grow. The overall picture is consistent with the following two premises: (i) the DW turbulence coupling to the turbulence-driven flow is a key trigger, (ii) the L-H transition is locked in by $V_E' \sim \nabla P_i / n$, i.e., by ion diamagnetic $E \times B$ shear.

Future work will focus on several topics, which include, but are not limited to:

(a) the effect of toroidal rotation and toroidal velocity shear on the threshold power,

(b) the impact of fueling by injection (i.e., pellets, SMBI, etc.),

(c) the effect of collisionless coupling and energy transfer by turbulence between electrons and ions on P_{thr}, in electron heating regimes. This is particularly relevant to ITER, and may also be relevant to strong ECH at low density.[44,45]

(d) the effect of energetic particles, which will introduce another energy channel,

(e) improved electron confinement regimes at low density where edge ∇T_e steepens more dramatically than edge ∇n.[27]

Item (c) is especially relevant to this paper. In collisionless regimes, electron-ion energy transfer mediated by drift wave turbulence can exceed collisional coupling.[44,45,49] The scalings of this transfer in density, temperature, and temperature gradient are predicted to be radically different from those of collisional coupling. Thus, the structure of the $P_{\text{thr}}(n)$ curve in ITER may differ significantly from that for present day tokamaks. Work on this important question is underway and will be discussed in future publications.

ACKNOWLEDGMENTS

[1]R. J. Groebner, D. R. Baker, K. H. Burrell, T. N. Carlstrom, J. R. Ferron, P. Gohil, L. L. Lao, T. H. Osborne, D. M. Thomas, W. P. West, J. A. Boedo, R. A. Moyer, G. R. McKee, R. D. Deranian, E. J. Doyle, C. L. Rettig, T. L. Rhodes, and J. C. Rost, Nucl. Fusion **41**, 1789 (2001).

[2]T. N. Carlstrom, R. J. Groebner, C. Fenzi, G. R. McKee, R. A. Moyer, and T. L. Rhodes, Plasma Phys. Controlled Fusion **44**, A333 (2002).

[3]E.-J. Kim and P. H. Diamond, Phys. Rev. Lett. **90**, 185006 (2003).

[4]P. H. Diamond, S.-I. Itoh, K. Itoh, and T. S. Hahm, Plasma Phys. Controlled Fusion **47**, R35 (2005).

[5]G. R. McKee, P. Gohil, D. J. Schlossberg, J. A. Boedo, K. H. Burrell, J. S. de Grassie, R. J. Groebner, R. A. Moyer, C. C. Petty, T. L. Rhodes, L. Schmitz, M. W. Shafer, W. M. Solomon, M. Umansky, G. Wang, A. E. White, and X. Xu, Nucl. Fusion **49**, 115016 (2009).

[6]G. D. Conway, C. Angioni, F. Ryter, P. Sauter, and J. Vicente, Phys. Rev. Lett. **106**, 065001 (2011).

[7]G. S. Xu, B. N. Wan, H. Q. Wang, H. Y. Guo, H. L. Zhao, A. D. Liu, V. Naulin, P. H. Diamond, G. R. Tynan, M. Xu, R. Chen, M. Jiang, P. Liu, N. Yan, W. Zhang, L. Wang, S. C. Liu, and S. Y. Ding, Phys. Rev. Lett. **107**, 125001 (2011).

[8]T. Estrada, C. Hidalgo, T. Happel, and P. H. Diamond, Phys. Rev. Lett. **107**, 245004 (2011).

[9]P. Gohil, T. E. Evans, M. E. Fenstermacher, J. R. Ferron, T. H. Osborne, J. M. Park, O. Schmitz, J. T. Scoville, and E. A. Unterberg, Nucl. Fusion **51**, 103020 (2011).

[10]K. Miki, P. H. Diamond, O. D. Gurcan, G. R. Tynan, T. Estrada, L. Schmitz, and G. S. Xu, Phys. Plasmas **19**, 092306 (2012).

[11]L. Schmitz, L. Zeng, T. L. Rhodes, J. C. Hillesheim, E. J. Doyle, R. J. Groebner, W. A. Peebles, K. H. Burrell, and G. Wang, Phys. Rev. Lett. **108**, 155002 (2012).

[12]T. Estrada, E. Ascasíbar, E. Blanco, A. Cappa, P. H. Diamond, T. Happel, C. Hidalgo, M. Liniers, B. P. van Milligen, I. Pastor, D. Tafalla, and the TJ-II Team, Plasma Phys. Controlled Fusion **54**, 124024 (2012).

[13]G. S. Xu, H. Q. Wang, B. N. Wan, H. Y. Guo, V. Naulin, P. H. Diamond, G. R. Tynan, M. Xu, N. Yan, W. Zhang, J. F. Chang, L. Wang, R. Chen, S. C. Liu, S. Y. Ding, L. M. Shao, H. Xiong, and H. L. Zhao, Phys. Plasmas **19**, 122502 (2012).

[14]I. Shesterikov, Y. Xu, G. R. Tynan, P. H. Diamond, S. Jachmich, P. Dumortier, M. Vergote, M. van Schoor, G. van Oost, and Textor Team, Phys. Rev. Lett. **111**, 055006 (2013).

[15]G. Tynan, M. Xu, P. Diamond, J. Boedo, I. Cziegler, N. Fedorczak, P. Manz, K. Miki, S. Thakur, L. Schmitz, L. Zeng, E. Doyle, G. McKee, Z. Yan, G. Xu, B. Wan, H. Wang, H. Guo, J. Dong, K. Zhao, J. Cheng, W. Hong, and L. Yan, Nucl. Fusion **53**, 073053 (2013).

[16]L. Schmitz, L. Zeng, T. L. Rhodes, J. C. Hillesheim, W. A. Peebles, R. J. Groebner, K. H. Burrell, G. R. McKee, Z. Yan, G. R. Tynan, P. H. Diamond, J. A. Boedo, E. J. Doyle, B. A. Grierson, C. Chrystal, M. E. Austin, W. M. Solomon, and G. Wang, Nucl. Fusion **54**, 073012 (2014).

[17]Z. Yan, G. R. McKee, R. Fonck, P. Gohil, R. J. Groebner, and T. H. Osborne, Phys. Rev. Lett. **112**, 125002 (2014).

[18]I. Cziegler, G. R. Tynan, P. H. Diamond, A. E. Hubbard, J. W. Hughes, J. Irby, and J. L. Terry, Plasma Phys. Controlled Fusion **56**, 075013 (2014).

[19]P. Manz, G. S. Xu, B. N. Wan, H. Q. Wang, H. Y. Guo, I. Cziegler, N. Fedorczak, C. Holland, S. H. Müller, S. C. Thakur, M. Xu, K. Miki, P. H. Diamond, and G. R. Tynan, Phys. Plasmas **19**, 072311 (2012).

[20]G. S. Xu, L. M. Shao, S. C. Liu, H. Q. Wang, B. N. Wan, H. Y. Guo, P. H. Diamond, G. R. Tynan, M. Xu, S. J. Zweben, V. Naulin, A. H. Nielsen, J. J. Rasmussen, N. Fedorczak, P. Manz, K. Miki, N. Yan, R. Chen, B. Cao, L. Chen, L. Wang, W. Zhang, and X. Z. Gong, Nucl. Fusion **54**, 013007 (2014).

[21]G. S. Xu, H. Q. Wang, M. Xu, B. N. Wan, H. Y. Guo, P. H. Diamond, G. R. Tynan, R. Chen, N. Yan, D. F. Kong, H. L. Zhao, A. D. Liu, T. Lan, V. Naulin, A. H. Nielsen, J. J. Rasmussen, K. Miki, P. Manz, W. Zhang, L. Wang, L. M. Shao, S. C. Liu, L. Chen, S. Y. Ding, N. Zhao, Y. L. Li, Y. L. Liu, G. H. Hu, X. Q. Wu, and X. Z. Gong, Nucl. Fusion **54**, 103002 (2014).

[22]K. Miki, P. H. Diamond, N. Fedorczak, Ö. D. Gürcan, M. Malkov, C. Lee, Y. Kosuga, G. Tynan, G. S. Xu, T. Estrada, D. McDonald, L. Schmitz, and K. J. Zhao, Nucl. Fusion **53**, 073044 (2013).

[23]Y. R. Martin and T. Takizuka, J. Phys. Conf. Ser. **123**, 012033 (2008).

[24]J. W. Connor and H. R. Wilson, Plasma Phys. Controlled Fusion **42**, R1 (2000).

[25]J. Snipes, R. Granetz, M. Greenwald, O. Kardaun, A. Kus, F. Ryter, U. Stroth, J. Kollermeyer, S. Fielding, M. Valovic, J. DeBoo, T. Carlstrom, D. Schissel, K. Thomsen, D. Campbell, J. Christiansen, J. Cordey, E. Righi, Y. Miura, N. Suzuki, M. Mori, T. Matsuda, H. Tamai, T. Fukuda, Y. Kamada, T. Matsuda, M. Sato, T. Takizuka, K. Tsuchiya, and S. Kaye, Nucl. Fusion **36**, 1217 (1996).

[26]C. F. Maggi, E. Delabie, T. M. Biewer, M. Groth, N. C. Hawkes, M. Lehnen, E. de la Luna, K. McCormick, C. Reux, F. Rimini, E. R. Solano, Y. Andrew, C. Bourdelle, V. Bobkov, M. Brix, G. Calabro, A. Czarnecka, J. Flanagan, E. Lerche, S. Marsen, I. Nunes, D. Van Eester, M. F. Stamp, and J. EFDA Contributors, Nucl. Fusion **54**, 023007 (2014).

[27]F. Ryter, L. B. Orte, B. Kurzan, R. McDermott, G. Tardini, E. Viezzer, M. Bernert, R. Fischer, and T. A. U. Team, Nucl. Fusion **54**, 083003 (2014).

[28]F. Ryter, S. Rathgeber, L. Barrera Orte, M. Bernert, G. Conway, R. Fischer, T. Happel, B. Kurzan, R. McDermott, a. Scarabosio, W. Suttrop, E. Viezzer, M. Willensdorfer, and E. Wolfrum, Nucl. Fusion **53**, 113003 (2013).

[29]E.-J. Kim and P. H. Diamond, Phys. Plasmas **10**, 1698 (2003).

[30]K. J. Zhao, J. Cheng, P. H. Diamond, J. Q. Dong, L. W. Yan, W. Y. Hong, M. Xu, G. Tynan, K. Miki, Z. H. Huang, K. Itoh, S.-I. Itoh, A. Fujisawa, Y. Nagashima, S. Inagaki, Z. X. Wang, L. Wei, X. M. Song, G. J. Lei, Q. Li, X. Q. Ji, Y. Liu, Q. W. Yang, X. T. Ding, X. R. Duan, and the HL-2A Team, Nucl. Fusion **53**, 123015 (2013).

[31]M. A. Malkov and P. H. Diamond, Phys. Plasmas **16**, 012504 (2009).

[32]M. Dam, M. Brøns, J. Juul Rasmussen, V. Naulin, and G. Xu, Phys. Plasmas **20**, 102302 (2013).

[33]H. Zhu, S. C. Chapman, R. O. Dendy, and K. Itoh, Phys. Plasmas **21**, 062307 (2014).

[34]K. Miki, P. H. Diamond, S. H. Hahn, W. W. Xiao, O. D. Gürcan, and G. R. Tynan, Phys. Rev. Lett. **110**, 195002 (2013).

[35]K. Miki, P. H. Diamond, S.-H. Hahn, W. W. Xiao, O. D. Gurcan, and G. R. Tynan, Phys. Plasmas **20**, 082304 (2013).

[36]P. Sauter, T. Pütterich, F. Ryter, E. Viezzer, E. Wolfrum, G. Conway, R. Fischer, B. Kurzan, R. McDermott, and S. Rathgeber, Nucl. Fusion **52**, 012001 (2012).

[37]A. E. Hubbard, D. G. Whyte, R. M. Churchill, A. Dominguez, J. W. Hughes, Y. Ma, E. S. Marmar, Y. Lin, M. L. Reinke, and A. E. White, Nucl. Fusion **52**, 114009 (2012).

[38]X. Garbet, N. Dubuit, E. Asp, Y. Sarazin, C. Bourdelle, P. Ghendrih, and G. T. Hoang, Phys. Plasmas **12**, 082511 (2005).

[39]P. Helander and D. J. Sigmar, *Collisional Transport in Magnetized Plasmas* (Cambridge University Press, 2005).

[40]P. Gohil, T. C. Jernigan, T. H. Osborne, J. T. Scoville, and E. J. Strait, Nucl. Fusion **50**, 064011 (2010).

[41]J. W. Hughes, A. Loarte, M. L. Reinke, J. L. Terry, D. Brunner, M. Greenwald, A. E. Hubbard, B. LaBombard, B. Lipschultz, Y. Ma, S. Wolfe, and S. J. Wukitch, Nucl. Fusion **51**, 083007 (2011).

[42]Y. Ma, J. W. Hughes, A. E. Hubbard, B. LaBombard, and J. Terry, Plasma Phys. Controlled Fusion **54**, 082002 (2012).

[43]B. Lloyd, Plasma Phys. Controlled Fusion **40**, A119 (1998).

[44]L. Zhao and P. H. Diamond, Phys. Plasmas **19**, 082309 (2012).

[45]X. Garbet, D. Esteve, Y. Sarazin, J. Abiteboul, C. Bourdelle, G. Dif-Pradalier, P. Ghendrih, V. Grandgirard, G. Latu, and A. Smolyakov, Phys. Plasmas **20**, 072502 (2013).

[46]M. A. Malkov, Sov. J. Plasma Phys. **6**, 1309 (1980).

[47]J. E. Rice, M. J. Greenwald, Y. A. Podpaly, M. L. Reinke, P. H. Diamond, J. W. Hughes, N. T. Howard, Y. Ma, I. Cziegler, B. P. Duval, P. C. Ennever, D. Ernst, C. L. Fiore, C. Gao, J. H. Irby, E. S. Marmar, M. Porkolab, N. Tsujii, and S. M. Wolfe, Phys. Plasmas **19**, 056106 (2012).

[48]P. Gohil, G. R. McKee, D. Schlossberg, L. Schmitz, and G. Wang, J. Phys. Conf. Ser. **123**, 012017 (2008).

[49]W. M. Manheimer, E. Ott, and W. M. Tang, Phys. Fluids **20**, 806 (1977).